90-518

сообщения
объединенного
института
ядерных
исследований
дубна

E2-90-518

G.V.Efimov, M.A.Ivanov, S.G.Mashnik*

ππ-SCATTERING IN THE QUARK CONFINEMENT MODEL. SCATTERING LENGTHS

*Institute of Applied Physics, Kishinev, USSR

1990

1. Introduction

This work continues the investigation [1] of the low—energy $\pi\pi$ – scattering in the Quark Confinement Model (QCM) [2]. In our approach, the $\pi\pi$ – scattering is described by the diagrams involving both the quark exchanges (box–diagrams) and the intermediate vector (ρ) and scalar (f_0 and ϵ) mesons (resonance diagrams). The set of scalar meson parameters was established which allows one to describe simultaneously the s - wave lengths a_0^0 and a_0^2 and the phases $\delta_0^0, \delta_2^0, \delta_1^1, \delta_3^1$, and the two–pion decay widths of scalar mesons with satisfactory accuracy.

The aim of this work is, first, to calculate the highest lengths of $\pi\pi$ – scattering (p, d, f and g) in the given approximation using the same scalar meson parameters and, second, to investigate the dependence of the obtained values on thes ones.

It was found that our results are in satisfactory agreement with the available experimental data and other approaches. The p, d, f and g wave lengths are found to decrease with increasing ϵ–meson mass m_ϵ. When $m_\epsilon \geq 700 MeV$ the values of a_2^2 and a_4^2 become negative. Experimentaly, the value a_2^2 is measured with large uncertainties. It was just established [3,4] that a_2^2 is small but the uncertainties of experimental data do not even allow one to determine the sign of it (see Fig.5). The wave length a_4^2 has not been measured yet. Our results allow one to conclude that if the wave lengths a_2^2 and a_4^2 will be found positive, then $m_\epsilon \approx 700 MeV$, otherwise, one can expect that $700 MeV < m_\epsilon \leq 800 MeV$.

2. $\pi\pi$-Scatering Lengths

The low-energy $\pi\pi$-scattering in the lowest order in $1/N_c$ - expansion is described by diagrams in Fig.1.

We use the standard Lagrangian [2] describing the meson–quark interaction

$$L_I = \frac{g_M}{\sqrt{2}} \sum_{i=0}^{8} M_i \bar{q} \Gamma_M \lambda^i q. \qquad (1)$$

Here, M_i are the Euclidean fields connected with the physical ones in a standard manner [2], λ^i are the Gell-Mann matrices ($\lambda^0 = \sqrt{\frac{2}{3}I}$), Γ_M are the Dirac matrices: $i\gamma^5$ for the pseudoscalar mesons ($P = \pi$), γ^μ for the vector ones ($V = \rho$), $I - i\frac{H}{\Lambda}\hat{\partial}$ for the scalar ones ($S = \epsilon, f_0$).

The mixing angles are defined as

$$\epsilon \longrightarrow cos\delta_S \frac{\bar{u}u + \bar{d}d}{\sqrt{2}} - sin\delta_S \bar{s}s;$$

$$f_0 \longrightarrow -sin\delta_S \frac{\bar{u}u + \bar{d}d}{\sqrt{2}} - cos\delta_S \bar{s}s;$$

$$\delta_S = \theta_S - \theta_I; \qquad sin\theta_I = \frac{1}{\sqrt{3}}.$$

The coupling constants g_M are defined by the compositeness condition (1.5). (Under quotations of the formulas, figures and appendices from the paper[1], we will use the auxiliary index 1.) It is convenient to use the effective coupling constants $h_M = 3g_M^2/4\pi^2$. Their expressions and numerical values are given in Appendix 1.1.

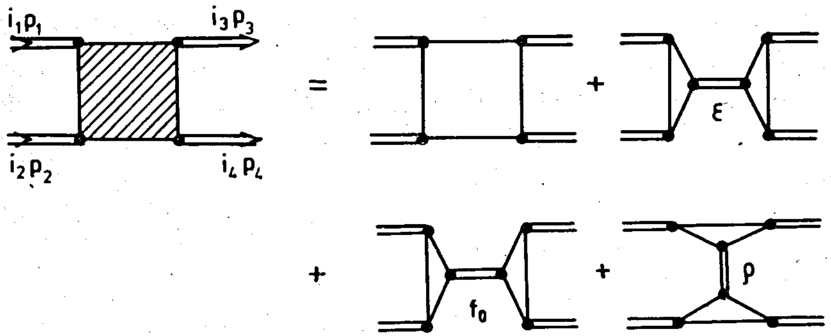

Fig.1. The diagrams defining the low-energy $\pi\pi$-scattering in one-loop approcximation (zero-order on $1/N_c$-expansion).

The role of the auxiliary term with a derivative in the scalar meson quark current was discussed in [1]. One has to remark that this term takes into account the complex structure of the scalar mesons in the phenomenological way. In this case, the auxiliary free parameter H appears. Moreover, the mixing angle δ_S and ϵ-meson mass m_ϵ are supposed to be free parameters. In the paper [1], the smooth dependences of H and

$sin\delta_S$ on the mass m_ϵ were found (Fig.2) which provided simultaneous description of a_0^0, a_0^2 and $\Gamma_{f_0 \to \pi\pi}$.

The value m_ϵ was determined from the best fit of the s-wave phase δ_0^0. It was found that $m_\epsilon \simeq 700 - 800 MeV$. Here, we will wse the obtained dependences H and $sin\delta_S$ on m_ϵ (see Fig.2) and calculate the scattering lengths for different values of m_ϵ.

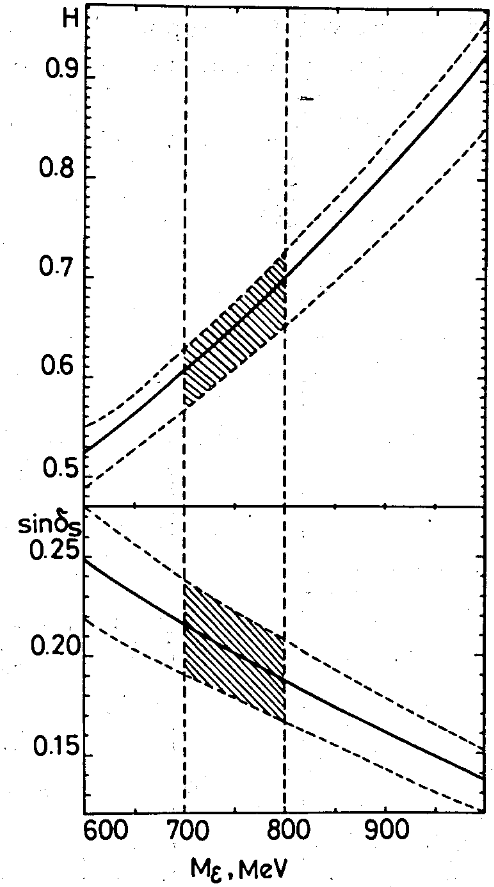

Fig.2. The dependences of H and $sin\delta_S$ on m_ϵ.

The scattering lengths a_l^I are defined in a standard manner[4]:

$$a_l^I = \frac{1}{m_\pi^{2l+1}} \lim_{s\to s_0} \left(\frac{s_0}{s-s_0}\right)^l A_l^I(s,t,u) =$$
$$= \frac{1}{m_\pi^{2l+1}} \lim_{s\to s_0} \left(\frac{s_0}{s-s_0}\right)^l \frac{1}{2}\int_{-1}^{1} dx P_l(x) A^I(s,t,u). \qquad (2)$$

Here A^I are the amplitudes with the isospin I; $P_l(x)$ are the Lagrange polynomials; $s_0 = 4m_\pi^2$; s, t, u are Mandelstam variables, such that

$$t = -\frac{1}{2}(s-s_0)(1-x)$$
$$u = -\frac{1}{2}(s-s_0)(1+x). \qquad (3)$$

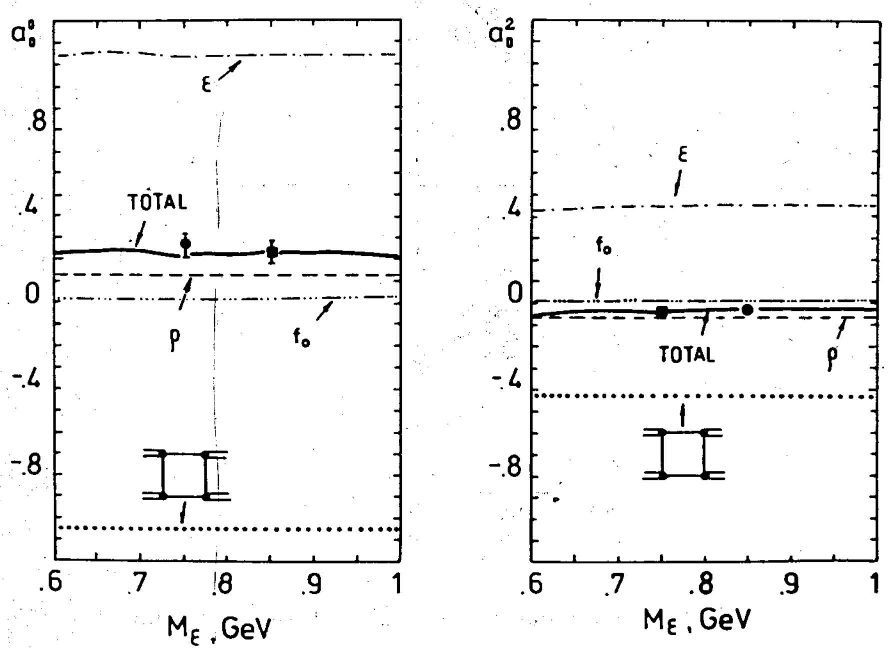

Fig.3. The comparison of the s-wave lengths a_0^0 and a_0^2 obtained in the QCM for different values of m_ε with the experimental data [3,4].

Both the contributions from separate diagrams and the total results are plotted.

Recalling the definition of the Lagrange polynomials

$$P_l(x) = \frac{1}{2^l l!}\frac{d^l}{dx^l}(x^2-1)^l$$

and using (3) and the formula

$$\frac{1}{2}\int_{-1}^{1} dx(1-x^2)^l = 2^{2l}\frac{l!l!}{(2l+1)!},$$

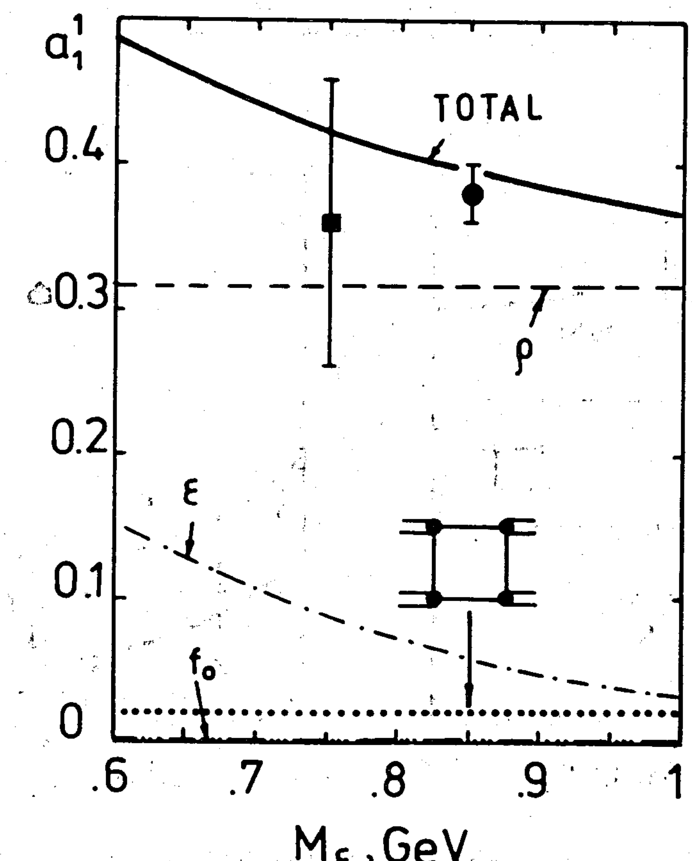

Fig.4. The p-wave length. The notation is the same as on Fig.3.

after l-multiple integration by parts expression (2) can be written in the form

$$
\begin{aligned}
m_\pi^3 a_1^1 &= \frac{s_0}{3!}\left(\frac{d}{du}-\frac{d}{dt}\right) A^1(s,t,u),\\
m_\pi^5 a_2^I &= \frac{2s_0^2}{5!}\left(\frac{d^2}{dt^2}-2\frac{d^2}{dtdu}+\frac{d^2}{du^2}\right) A^I(s,t,u),\\
m_\pi^7 a_3^1 &= \frac{3!s_0^3}{7!}\left(\frac{d^3}{dt^3}-3\frac{d^3}{dt^2du}+3\frac{d^3}{dtdu^2}-\frac{d^3}{du^3}\right) A^1(s,t,u),\\
m_\pi^9 a_4^I &= \frac{4!s_0^4}{9!}\left(\frac{d^4}{dt^4}-4\frac{d^4}{dt^3du}+6\frac{d^4}{dt^2du^2}-4\frac{d^4}{dtdu^3}+\frac{d^4}{du^4}\right) A^I(s,t,u),
\end{aligned}
\tag{4}
$$

for $s=s_0$, $t=u=0$.

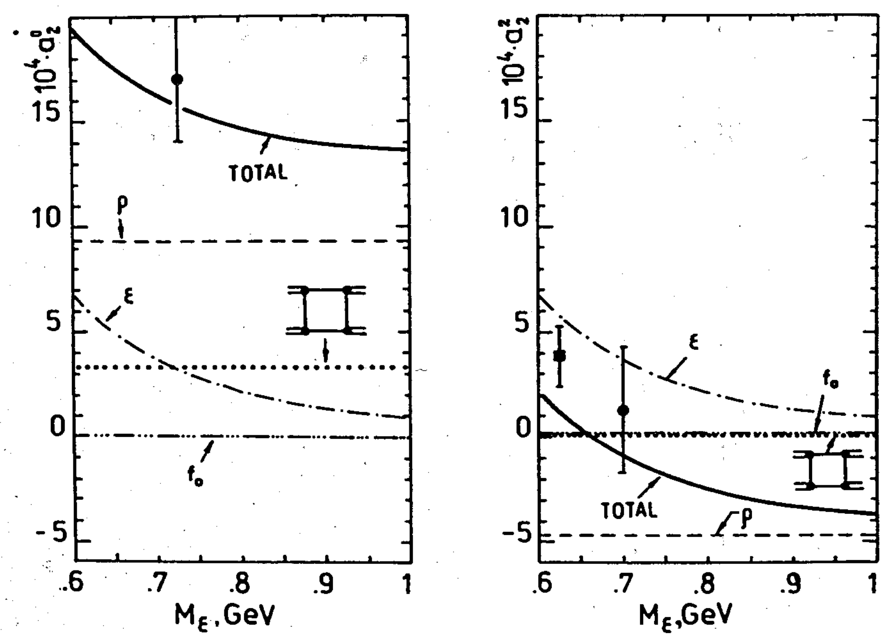

Fig.5. The d-wave lengths. The notation is the same as on Fig.3.

After the standard calculation[2] we have the following expressions for the $\pi\pi$-scattering amplitudes with the isospin I

$$
\begin{aligned}
A^0(s,t,u) &= 3A(s,t,u)+A(t,s,u)+A(u,t,s)=\\
&= \frac{1}{32\pi}\{-[3G_\Box(s,t,u)+G_\Box(t,s,u)+G_\Box(u,t,s)]+\\
&+ [3G^2_{\epsilon\pi\pi}(s)D_\epsilon(s)+G^2_{\epsilon\pi\pi}(t)D_\epsilon(t)+G^2_{\epsilon\pi\pi}(u)D_\epsilon(u)]+\\
&+ [3G^2_{f_0\pi\pi}(s)D_{f_0}(s)+G^2_{f_0\pi\pi}(t)D_{f_0}(t)+G^2_{f_0\pi\pi}(u)D_{f_0}(u)]+\\
&+ 2[(s-u)G^2_{\rho\pi\pi}(t)D_\rho(t)+(s-t)G^2_{\rho\pi\pi}(u)D_\rho(u)]\} \equiv\\
&\equiv A^0_\Box(s,t,u)+A^0_\epsilon(s,t,u)+A^0_{f_0}(s,t,u)+A^0_\rho(s,t,u);
\end{aligned}
\tag{5}
$$

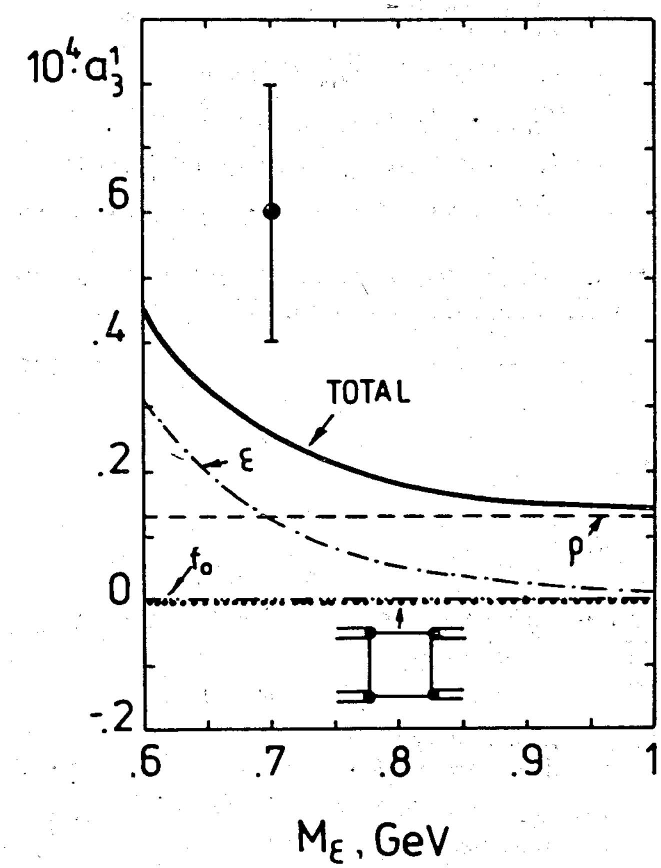

Fig.6. The f-wave length. The notation is the same as on Fig.3.

$$
\begin{aligned}
A^1(s,t,u) &= A(t,s,u) - A(u,t,s) = \qquad (6)\\
&= \frac{1}{32\pi}\{-[G_\Box(t,s,u) - G_\Box(u,t,s)] + \\
&+ [G^2_{\epsilon\pi\pi}(t)D_\epsilon(t) - G^2_{\epsilon\pi\pi}(u)D_\epsilon(u)] + \\
&+ [G^2_{f_0\pi\pi}(t)D_{f_0}(t) - G^2_{f_0\pi\pi}(u)D_{f_0}(u)] + \\
&+ [(s-u)G^2_{\rho\pi\pi}(t)D_\rho(t) - (s-t)G^2_{\rho\pi\pi}(u)D_\rho(u) + \\
&+ 2(t-u)G^2_{\rho\pi\pi}(s)D_\rho(s)]\} \equiv \\
&\equiv A^1_\Box(s,t,u) + A^1_\epsilon(s,t,u) + A^1_{f_0}(s,t,u) + A^1_\rho(s,t,u);
\end{aligned}
$$

$$
\begin{aligned}
A^2(s,t,u) &= A(t,s,u) + A(u,t,s) = \qquad (7)\\
&= \frac{1}{32\pi}\{-[G_\Box(t,s,u) + G_\Box(u,t,s)] + \\
&+ [G^2_{\epsilon\pi\pi}(t)D_\epsilon(t) + G^2_{\epsilon\pi\pi}(u)D_\epsilon(u)] + \\
&+ [G^2_{f_0\pi\pi}(t)D_{f_0}(t) + G^2_{f_0\pi\pi}(u)D_{f_0}(u)] - \\
&- [(s-u)G^2_{\rho\pi\pi}(t)D_\rho(t) + (s-t)G^2_{\rho\pi\pi}(u)D_\rho(u)]\} \equiv \\
&\equiv A^2_\Box(s,t,u) + A^2_\epsilon(s,t,u) + A^2_{f_0}(s,t,u) + A^2_\rho(s,t,u).
\end{aligned}
$$

The functions $G_\Box$, $G_{\epsilon\pi\pi}$, $G_{f_0\pi\pi}$, $G_{\rho\pi\pi}$ are shown in Appendix 1.2 and the propagators $D_{\epsilon,f_0,\rho}$ are defined by formulas (1.8) and (1.9).

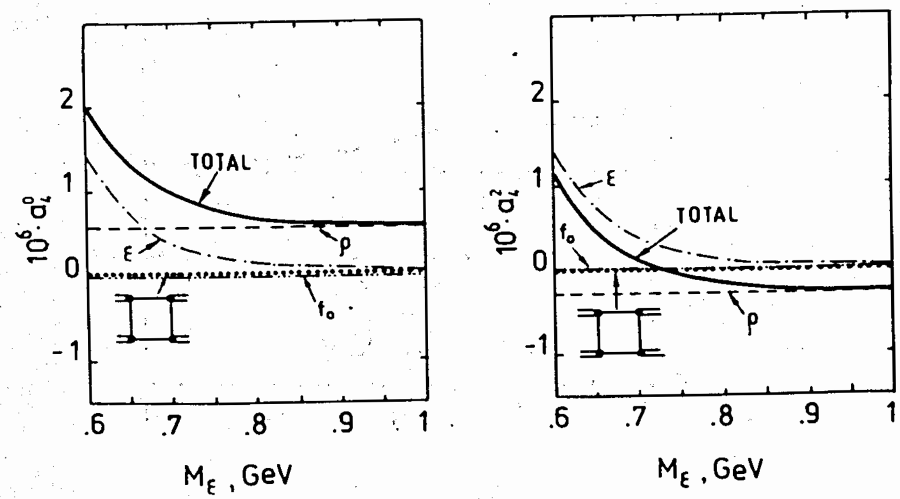

Fig.7. The g-wave lengths. The notation is the same as on Fig.3.

Substituing (5-7) into (4), we obtain the final expressions for the scattering lengths ($l > 0$) which are shown in Appendix. The s-wave lengths a^0_0 and a^2_0 are defined by (1.13).

The numerical results of the lengths a^I_l (units $m_\pi = 0$) are shown in Figs.3-7 and the Table. They also show experimental data and results of other approaches.

Table

The comparison of the lengths a^I_l obtained in the QCM with the available experimental data and other approaches.

a^I_l	Experiment [3],[4]	*QCM* $m_\epsilon = 650$ MeV	*QCM* $m_\epsilon = 750$ MeV	[5] $m_\epsilon = 730$ MeV	[6]
a^0_0	0.26 ± 0.05 0.23 ± 0.05	0.233	0.228	0.26	0.22
a^2_0	-0.028 ± 0.012 -0.05 ± 0.03	-0.049	-0.034	-0.05	-0.05
a^1_1	0.038 ± 0.002 0.036 ± 0.010	0.046	0.041	0.04	0.039
$10^4 \cdot a^0_2$	17 ± 3	17.7	14.8	15	17
$10^4 \cdot a^2_2$	1.3 ± 3.0 3.8 ± 1.4	0.316	-2.53	3	1.6
$10^4 \cdot a^1_3$	0.6 ± 0.2	0.323	0.183	0.4	
$10^6 \cdot a^0_4$		1.31	0.695		
$10^6 \cdot a^2_4$		0.428	-0.188		

One can see, our results are in a quite reasonable agreement with the available experimental data and other approaches.

To ascertain the sensibility of the calculated in the QCM scattering lengths a^I_l on the scalar mesons parameters H , $sin\delta_S$ and m_ϵ we have made the corresponding numerical calculations. It was found that

i) On the values of H the most sensible are the s-wave lengths a^0_0 and a^2_0. a^0_0 and a^2_0 increase approximately twice with increasing H inside the corresponding interval for each input value of m_ϵ (see Fig.2); a^2_2 increases in this case by $\approx 30\%$ and the rest a_l^I are practically insensitive to such changes of H.

ii) a_0^0 , a_0^2 and a_2^2 decrease by $\approx 15\%$ with increasing $sin\delta_S$ inside the corresponding interval for each input value of m_ϵ (see Fig.2). The rest a_l^I are practically insensitive to such changes of $sin\delta_S$.

iii) All the scattering lengths except a_0^0 and a_0^2, to which in [1] the dependenses of H and $sin\delta_S$ on m_ϵ have been fitted , decrease with increasing ϵ-meson mass m_ϵ (see Fig.4-7).

Let us make some remarks concerning the relative contributions of different diagrams (see Fig.1). From Fig.3-7 one can see that the resonance diagrams with f_0 scalar mesons give the least contribution for any a_l^I. It is the result of the small $f_0 \to \pi\pi$ decay width $\Gamma_{f_0\to\pi\pi}$ (see Fig.1.6). From Fig.3 one can see that for a_0^0 and a_0^2 the contributions of box diagrams cancel the contributions of diagrams with ϵ mesons only partially but not completely as in the σ-model. Diagrams with vector ρ mesons give contributions in all a_l^I. The contributions of diagrams with ϵ mesons for a_l^I $(l > 0)$ decrease with increasing m_ϵ , and accordingly, the relative contributions of diagrams with ρ mesons increase. As $a_l^{I=2}(\rho) < 0$, the theoretical values of a_2^2 and a_4^2 become negative when $m_\epsilon \geq 700$ MeV (see Fig.5,7). Such a behaviour of theoretical a_2^2 and a_4^2 allows one to draw a qualitative conclusion about the value of ϵ-meson mass m_ϵ. Experimentally, the value a_2^2 is measured with large uncertainties. It was just established [3,4] that a_2^2 is small but the uncertainties of experimental data do not even allow to determine its sign (see Fig.5). The wave length a_4^2 has not been measured yet. Our results allow one to conclude that if in the future precision experiments the wave lenghs a_2^2 and a_4^2 are found positive, then $m_\epsilon \leq 700$ MeV. Taking into account the preferable interval $m_\epsilon \in$ (700-800) MeV found in [1], we can conclude that $m_\epsilon \approx$ 700 MeV, otherwise, one can expect that $700MeV < m_\epsilon \leq 800MeV$.

3. Discussion

Thus, all presently measured $\pi\pi$-scattering lengths a_l^I are satisfactorily described here in the framework of the QCM by taking into account only the "lower diagrams", i.e. the box-diagrams and the intermediate vector (ρ) and scalar (f_0 and ϵ) meson exchanges (see Fig.1).

We consider our results as preliminary ones. So, in this work we

have not taken into account the tensor $f_2(1270)$, the scalar $f_0(1400)$ and other heavier meson exchanges, which are important in $\pi\pi$- scattering at energies$\sqrt{s} > 1$ GeV. Further, it is known (see, for example [6]) that in the chiral theory the pion-loop diagrams give an essential contribution to the $\pi\pi$-scattering amplitudes. In the QCM the rescattering diagrams, Fig.1.3, correspond to the pion-loop ones. Such diagrams have also been neglected here.

Apparently, the "higher diagrams" disregarded here are important in the description of $\pi\pi$-scattering at energies$\sqrt{s} \geq 1$ GeV, and we are going to solve this problem in our next paper. The fact that we described here with satisfactory accuracy all the currently measured $\pi\pi$-scattering lengths a_l^I, and in [1] the phase shifts δ_0^0, δ_2^0, δ_1^1, δ_3^1 and the two-pion decay widths of scalar mesons using a fixed set of model parameters and taking into account only the "lower diagrams", allows us to assume that the latter ones are determinative in the region$\sqrt{s} \leq 900$ MeV. One can expect that the inclusion of the "higher diagrams" in the description of $\pi\pi$-scattering lengths and pase shifts in the region$\sqrt{s} \leq 900$ MeV will lead to some nonessential changes of obtained here and in [1] numerical values, but will not change our main results, in particular, the conclusion regarding the existence of the broad scalar ϵ (700-800)-resonance.

We wish to thank M.K.Volkov and S.B.Gerasimov for fruitful discussions of the subject treated in this paper.

Appendix

$$m_\pi^3 a_1^1(\Box) = \frac{\pi h_\pi^2 s_0}{1152\Lambda^2}\left\{-\frac{2}{3}b(0) + \frac{s_0}{6\Lambda^2}b'(0) + I_1^\Box\right\},$$

$$I_1^\Box = \int_0^1 dx b\left(-\frac{x s_0}{4\Lambda^2}\right) ln\frac{1+\sqrt{1-x}}{1-\sqrt{1-x}}, \qquad \Lambda = 460MeV.$$

$$m_\pi^3 a_1^1(s) = \frac{\pi h_\pi^2 m_\pi^2}{864\Lambda^2}\cdot\Lambda^2 D_S(0)\cdot C_{S\pi\pi}^2 F_H[\Lambda^2 D_S(0)\cdot 3F_H R(0) - 2],$$

$$s \equiv \epsilon, f_0; \qquad F_H = A_0 - 4HB_1$$

$$m_\pi^3 a_1^1(\rho) = \frac{\pi h_\pi^2 s_0}{72\Lambda^2}\left\{\Lambda^2 D_\rho(s_0)\left(B_0 + \frac{m_\pi^2 I_0}{\Lambda^2}\right)^2 + \right.$$

$$+\Lambda^2 D_\rho(0)\left[\frac{B_0^2}{4}+\frac{s_0B_0[2+\Lambda^2D_\rho(0)B_0^2]}{12\Lambda^2}\right]\Bigg\},$$

$$I_0=\int_0^1 dx\, b\left(-\frac{xs_0}{4\Lambda^2}\right)\sqrt{1-x}.$$

$$A_n=\int_0^\infty dt\, t^n a(t);\qquad B_n=\int_0^\infty dt\, t^n b(t).$$

The confinement functions $a(t)$ and $b(t)$ are defined by the formula (1.2). The structure functions R and $C_{S\pi\pi}$ are shown in Appendix 1.2.

$$m_\pi^5 a_2^2(\Box)=\frac{\pi h_\pi^2}{90}\left(\frac{m_\pi}{\Lambda}\right)^4\times 0.006666.$$

$$m_\pi^5 a_2^2(s)=\frac{\pi h_\pi^2}{32400}\left(\frac{m_\pi}{\Lambda}\right)^4 C_{S\pi\pi}^2\cdot\Lambda^2 D_S(0)\{5-3F_H(1+2H)+$$

$$+\Lambda^2 D_S(0)\cdot 6F_H[3F_H(1+4H)-5R(0)]+\Lambda^4D_S^2(0)\cdot 45F_H^2R^2(0)\}.$$

$$m_\pi^5 a_2^2(\rho)=-\frac{\pi h_\pi^2}{135}\left(\frac{m_\pi}{\Lambda}\right)^4 B_0\cdot\Lambda^2 D_\rho(0)\left\{\left(2+\frac{s_0}{3B_0\Lambda^2}-\frac{2s_0}{25\Lambda^2}\right)+\right.$$

$$\left.+\Lambda^2D_\rho(0)B_0\left(B_0+\frac{16s_0}{15\Lambda^2}\right)+\Lambda^4D_\rho^2(0)\frac{s_0B_0^3}{3\Lambda^2}\right\}.$$

$$m_\pi^5 a_2^0(\Box)=m_\pi^5 a_2^2(\Box)-\frac{\pi h_\pi^2}{30}\left(\frac{m_\pi}{\Lambda}\right)^4(0.02373-0.36524\cdot I_2^\Box);$$

$$I_2^\Box=\int_0^1 dx\int_0^{1-x}dy\int_0^{1-x-y}dz\cdot yz(1-x-y-z)b''\left(-\frac{xzs_0}{\Lambda^2}\right).$$

$$a_2^0(\rho)=-2a_2^2(\rho).$$

$$a_2^0(s)=a_2^2(s).$$

$$m_\pi^7 a_3^1(\Box)=\frac{\pi h_\pi^2}{315}\left(\frac{m_\pi}{\Lambda}\right)^6(0.0124+3I_3^\Box);$$

$$I_3^\Box=\int_0^1 dx\int_0^{1-x}dy\int_0^{1-x-y}dz\cdot xz^2b''\left(-\frac{ys_0(1-x-y-z)}{\Lambda^2}\right).$$

$$m_\pi^7 a_3^1(s)=\frac{\pi h_\pi^2}{1260}\left(\frac{m_\pi}{\Lambda}\right)^6 C_{S\pi\pi}^2\cdot\Lambda^2D_S(0)\left\{\frac{1+2H}{60}+\frac{F_H(5+8H)}{1050}+\right.$$

$$+\Lambda^2D_S(0)\left[\frac{R(0)}{12}-\frac{R(0)F_H(1+2H)}{20}-\frac{F_H(1+4H)}{5}-\right.$$

$$\left.-\frac{3F_H^2(1-10H-10H^2)}{175}\right]+$$

$$\left.+\Lambda^4D_S^2(0)\left[\frac{3R(0)F_H(1+4H)}{5}-\frac{R^2(0)F_H}{2}\right]+\Lambda^6D_S^3(0)\frac{3R^3(0)F_H^2}{4}\right\}.$$

$$m_\pi^7 a_3^1(\rho)=\frac{\pi h_\pi^2}{315}\left(\frac{m_\pi}{\Lambda}\right)^6\Lambda^2D_\rho(0)\left\{\frac{s_0}{\Lambda^2}\left[-\frac{420+414B_0}{7875}+\right.\right.$$

$$\left.+\Lambda^2D_\rho(0)\frac{B_0(1190-138B_0)}{1575}+\Lambda^4D_\rho^2(0)\frac{92B_0^3}{135}+\Lambda^6D_\rho^3(0)\frac{2B_0^5}{9}\right]+$$

$$\left.+\frac{50-12B_0}{75}+\Lambda^2D_\rho(0)\frac{32B_0}{15}+\Lambda^4D_\rho^2(0)\frac{2B_0^4}{3}\right\}.$$

$$m_\pi^9 a_4^2(\Box)=-\frac{2\pi h_\pi^2}{2835}\left(\frac{m_\pi}{\Lambda}\right)^8(0.010957+6I_4^\Box);$$

$$I_4^{\Box} = \int_0^1 dx \int_0^{1-x} dy \int_0^{1-x-y} dz \cdot x^2 z^3 b''' \left(-\frac{y s_0 (1-x-y-z)}{\Lambda^2}\right).$$

$$m_\pi^9 a_4^2(s) = \frac{\pi h_\pi^2}{5670}\left(\frac{m_\pi}{\Lambda}\right)^8 C_{S\pi\pi}^2 \Lambda^2 D_S(0)\left\{\frac{1+2H}{600} - \frac{5+8H}{1575} + \right.$$
$$+\frac{F_H(125+276H)}{31500}+$$
$$+\Lambda^2 D_S(0)\left[R(0)\left(\frac{F_H(5+8H)}{525}+\frac{1+2H}{30}\right)-\right.$$
$$-\frac{F_H^2(1219+3975H+6360H^2)}{15750}+$$
$$\left.+\frac{1+4H}{15}-\frac{F_H(3+82H+96H^2)}{175}\right]+$$
$$+\Lambda^4 D_S^2(0)\left[R^2(0)\left(\frac{1}{6}-\frac{F_H(1+2H)}{10}\right)-\frac{4R(0)F_H(1+4H)}{5}+\right.$$
$$\left.+\frac{6F_H^2(5+76H+132H^2)}{175}\right]+$$
$$\left.+\Lambda^6 D_S^3(0)\left[-R^3(0)F_H+\frac{9R^2(0)F_H^2(1+4H)}{5}\right]+\Lambda^8 D_S^4(0)\frac{3R^4(0)F_H^2}{2}\right\},$$

$$m_\pi^9 a_4^2(\rho) = -\frac{2\pi h_\pi^2}{2835}\left(\frac{m_\pi}{\Lambda}\right)^8\left\{\frac{s_0}{\Lambda^2}\left[\Lambda^2 D_\rho(0)\left(-\frac{864}{13125}+\frac{584B_0}{39375}\right)+\right.\right.$$
$$+\Lambda^4 D_\rho^2(0)\left(\frac{64}{225}-\frac{1512}{6125}B_0+\frac{4}{315}B_0^2\right)+$$
$$+\Lambda^6 D_\rho^3(0)\left(\frac{9848}{14175}B_0^2-\frac{220}{1575}B_0^3\right)+$$
$$\left.+\Lambda^8 D_\rho^4(0)\cdot\frac{16}{15}B_0+\Lambda^{10}D_\rho^5(0)\cdot\frac{8}{27}B_0^6\right]+$$
$$+4\left[-\Lambda^2 D_\rho(0)\frac{278}{2625}+\Lambda^4 D_\rho^2(0)\left(\frac{306}{405}B_0-\frac{46}{525}B_0^2\right)+\right.$$

$$\left.\left.+\Lambda^6 D_\rho^3(0)\frac{44}{45}B_0^3+\Lambda^8 D_\rho^4(0)\cdot\frac{2}{9}\right]\right\}.$$

$$m_\pi^9 a_4^0(\Box) = m_\pi^9 a_4^2(\Box) + (0.001797 + 0.251437 I_5^{\Box})\cdot 10^{-6},$$

$$I_5^{\Box} = \int_0^1 dx \int_0^{1-x} dy \int_0^{1-x-y} dz \cdot y^3 z (1-x-y-z)^3 b'''' \left(-\frac{x z s_0}{\Lambda^2}\right).$$

$$a_4^0(s) = a_4^2(s).$$

$$a_4^0(\rho) = -2a_4^2(\rho).$$

The numerical results showed in Fig.3-7 and in the Table were obtained by using the following values of H and $sin\delta_S$ (see Fig.2).

m_ϵ GeV	.6	.65	.70	.75	.80	.85	.90	.95	1.00
H	.532	.574	.618	.660	.711	.763	.820	.880	.940
$sin\delta_S$	.230	.210	.200	.190	.175	.160	.150	.140	.130

References

[1] G.V.Efimov, M.A.Ivanov, S.G.Mashnik, JINR, E2-89-780, Dubna, 1989.

[2] G.V.Efimov, M.A.Ivanov, Int.J.of Mod.Phys., 1989, A4, 2031.

[3] O.Dumbrajs et al., Nucl.Phys., 1983, B216, 277.

[4] A.A.Bel'kov et al. Pion-Pion Interaction, M., "Energoatomizdat", 1985.

[5] M.K.Volkov, Particles and Nuclei, 1986, 17, 433.

[6] A.A.Bel'kov, V.N.Pervushin, D.Ebert, JINR, P2-88-656, Dubna, 1988.

Received by Publishing Department
on November 13, 1990.